remote sensing

MDPI

Article

Towards the Combination of C2RCC Processors for Improving Water Quality Retrieval in Inland and Coastal Areas

Jesús Soriano-González [1,2,*], Esther Patricia Urrego [3], Xavier Sòria-Perpinyà [3], Eduard Angelats [1], Carles Alcaraz [2], Jesús Delegido [3], Antonio Ruíz-Verdú [3], Carolina Tenjo [3], Eduardo Vicente [4] and José Moreno [3]

1 Geomatics Research Unit, Centre Tecnològic de Telecomunicacions de Catalunya (CTTC/CERCA), Av. Gauss 7, 08860 Castelldefels, Barcelona, Spain; eduard.angelats@cttc.cat
2 IRTA Marine and Continental Waters, Carretera Poble Nou Km 5.5, 43540 La Ràpita, Tarragona, Spain; carles.alcaraz@irta.cat
3 Image Processing Laboratory, Laboratory of Earth Observation, Universität de València, C/Catedrático José Beltrán 2, 46980 Valencia, Spain; patricia.urrego@uv.es (E.P.U.); javier.soria-perpina@uv.es (X.S.-P.); jesus.delegido@uv.es (J.D.); antonio.ruiz@uv.es (A.R.-V.); carolina.tenjo@uv.es (C.T.); jose.moreno@uv.es (J.M.)
4 Institut Cavanilles de Biodiversitat i Biología Evolutiva, Universitat de València, C/Catedrático José Beltrán 2, 46980 Valencia, Spain; eduardo.vicente@uv.es
* Correspondence: jesus.soriano@cttc.cat

Abstract: Sentinel-2 offers great potential for monitoring water quality in inland and coastal waters. However, atmospheric correction in these waters is challenging, and there is no standardized approach yet, but different methods coexist under constant development. The atmospheric correction Case 2 Regional Coast Colour (C2RCC) processor has been recently updated with the C2X-COMPLEX (C2XC). This study is one of the first attempts at exploring its performance, in comparison with C2RCC and C2X, in inland and coastal waters in the east of the Iberian Peninsula, in retrieving water surface reflectance and estimating chlorophyll-a ([Chl-*a*]), total suspended matter ([TSM]), and Secchi disk depth (Z_{SD}). The relationship between in situ Z_{SD} and Kd_z90max product (i.e., the depth of the water column from which 90% of the water-leaving irradiance is derived) of the C2RCC processors demonstrated the potential of this product for estimating water clarity ($r > 0.75$). However, [TSM] and [Chl-*a*] derived from the different processors with default calibration factors were not suitable within the targeted scenarios, requiring recalibration based on optical water types or a shift to dynamic algorithm blending approaches. This would benefit from switching between C2RCC and C2XC, which extends the potential for improving surface reflectance estimates to a wide range of scenarios and suggests a promising future for C2-Nets in operational monitoring of water quality.

Keywords: Sentinel-2; atmospheric correction; validation; C2X-COMPLEX; water quality

check for updates

Citation: Soriano-González, J.; Urrego, E.P.; Sòria-Perpinyà, X.; Angelats, E.; Alcaraz, C.; Delegido, J.; Ruíz-Verdú, A.; Tenjo, C.; Vicente, E.; Moreno, J. Towards the Combination of C2RCC Processors for Improving Water Quality Retrieval in Inland and Coastal Areas. *Remote Sens.* **2022**, *14*, 1124. https://doi.org/10.3390/rs14051124

Academic Editor: Teodosio Lacava

Received: 14 January 2022
Accepted: 22 February 2022
Published: 24 February 2022

Publisher's Note: MDPI stays neutral with regard to jurisdictional claims in published maps and institutional affiliations.

Copyright: © 2022 by the authors. Licensee MDPI, Basel, Switzerland. This article is an open access article distributed under the terms and conditions of the Creative Commons Attribution (CC BY) license (https://creativecommons.org/licenses/by/4.0/).

1. Introduction

The quality of inland and coastal waters is increasingly threatened by human-driven activities and climate change [1], requiring timely and accurate information on the water quality parameters to understand ecosystem dynamics [2] and achieve the Sustainable Development Goals [3]. Water quality involves the measurement of the concentration of many parameters, including phytoplankton biomass, total suspended matter, and water transparency. These are key indicators of changes in the water column that provide valuable information on, for instance, the trophic and ecological status, the nutrient surplus, and the particulate load in the water column [4]. Due to the high spatiotemporal variability, water quality monitoring requires frequent, global, and systematic measurements.

Accomplishing these demands, the new generation of Earth observation satellites such as Landsat and Sentinels constellations provide free systematic data with enhanced radiometric, spatial, and temporal resolutions with respect to the previous generation of

Earth observation satellites. In particular, the Sentinel-2 satellites (S2A and S2B) operated by the European Space Agency (ESA) have opened up new potential for monitoring water quality in a wide range of geographical scopes [5,6]. However, achieving realistic and systematic water reflectance and, thus, water quality estimates from satellite remote sensing is challenging. Low reflectance of water in the visible–near infrared (VIS–NIR) regions of the spectrum [7] prevents water-leaving reflectance from reaching more than 20% of the total reflectance sensed at the top of the atmosphere (TOA), while atmospheric contribution can reach up to 90% [8]. Correcting the contribution of atmospheric constituents (such as gases and aerosols) in the captured images (radiance at the satellite sensor) for each date and location is a major issue in remote sensing of aquatic environments. Atmospheric correction is also challenged by additional effects such as the presence of sun glint (specular reflection of sunlight over water) or land adjacency (radiance from surrounding land affecting closest water pixels), which are complex to estimate and site-specific [9]. In coastal and inland waters these effects are frequently coupled with high variability and low covariance in optically active constituents. In these waters, classified as case-2, the inorganic and/or organic sediments make an important or dominant contribution to the optical properties [10], requiring high accuracy and precision in the atmospheric correction algorithms to successfully retrieve water constituents.

Atmospheric correction in case-2 waters has not been solved yet. As a result, huge efforts have been made to develop atmospheric correction processors, covering a wide range of different methods [11–13]. However, the performance of the processors may differ depending on the scenario (sun and observation geometry, atmospheric, optical, and site-specific conditions), and there is no standardized approach yet, but atmospheric correction processors keep evolving as new approaches and more data become available. This makes it necessary to continue validating different atmospheric correction approaches as well as water quality retrieval methods with in situ data accounting for a wide variety of water types and environmental conditions.

The atmospheric correction Case 2 Regional Coast Colour (C2RCC) processor has been updated. The C2RCC is a development of the original Case 2 Regional processor [14] adapted to different multispectral satellites (e.g., Sentinel-2, Landsat-8). The most recent update (available since February 2021) includes a new processor trained for atmospheric correction in complex waters. The C2RCC thus currently accounts for three processors (i.e., C2-Nets: C2RCC, C2X, and C2X-COMPLEX) using different training datasets within a neural network (NN) approach.

This study focuses on the validation of the remote sensing reflectance and key water quality parameters retrieved from Sentinel-2 Multispectral Imagery (S2-MSI) processed with the different C2-Nets. The validation datasets include in situ measurements of above-water radiometry (bottom of atmosphere reflectance, BOA), chlorophyll-a concentration ([Chl-*a*]) data as an indicator of phytoplankton biomass, total suspended matter ([TSM]) as an indicator of particulate load, and Secchi disk depth (Z_{SD}) measurements related to water transparency. The study areas comprise a set of 12 different inland reservoirs and transitional and coastal waters at the Eastern Iberian Peninsula (Spain). The objectives of the study were to: (i) assess and compare the performance of C2-Nets for atmospheric correction of case-2 waters; (ii) validate C2-Nets-derived water quality products (i.e., [Chl-*a*], [TSM], and Z_{SD}); (iii) define potential use cases and main constraints for C2-Nets-based operational water quality monitoring.

2. Materials and Methods

2.1. Study Areas

Ten freshwater reservoirs (ca. 1 PSU), a coastal bay (Alfacs bay, ca. 35 PSU), and Pétrola, an endorheic saline lagoon (ca. 60 PSU) were included in this study (Figure 1); all of them are located in the Eastern Iberian Peninsula (Spain). The study areas have different altitudes with respect to the sea level and include diverse morphological and biophysical characteristics, covering a wide variety of trophic states (Table 1). The monitoring of water

quality in these areas is challenging for remote sensing due to the complex and variable characteristics of these environments (e.g., high spatiotemporal variability, small, shallow waters, and land adjacency effects).

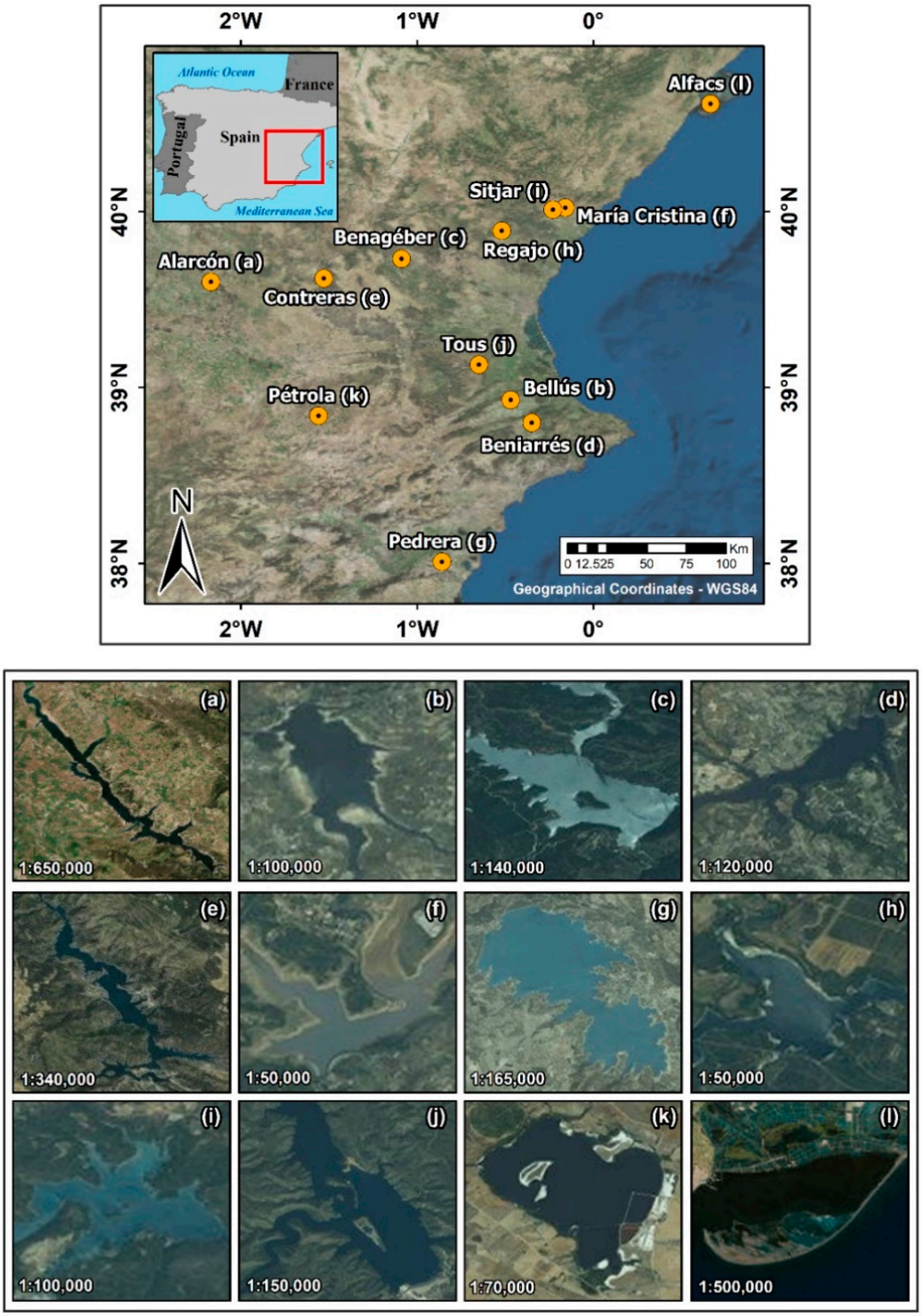

Figure 1. Study areas. Basemap source: Esri, DigitalGlobe, GeoEye, Earthstar Geographics, CNES/AIRbus DS, USDA, USGS, AeroGrid, IGN, and GIS User community.

Table 1. Descriptors of study areas by location, including the number of valid S2 images and in situ measurements (N_{xxx}), the altitude (elevation), surface, salinity, and the ranges within S2 dates of atmospheric pressure, ozone (O_3), [Chl-*a*], [TSM], and Z_{SD}.

Location	N_{Dates}	Elevation (m)	Surface (km^2)	Salinity (PSU)	Pressure (hPa)	O_3 (DU)	$N_{Radiometry}$	$N_{[Chl\text{-}a]}$	[Chl-*a*] (mg/m^3)	N_{TSM}	[TSM] (g/m^3)	N_{ZSD}	Z_{SD} (m)
Alarcón	2	814	68.4	1	[1014.1–1016.64]	[247–252]	10	10	[1.1–5.26]	-	-	10	[1.75–4.6]
Bellús	3	159	8	1	[1006.14–1007.85]	[251–252]	6	6	[13.86–68.01]	6	[18.66–22.13]	6	[0.45–0.63]
Benagéber	2	530	12	1	[1011.38–1011.74]	[249–277]	7	6	[2.49–12.40]	6	[1.82–2.72]	6	[4–7.7]
Beniarrés	2	321	2.6	1	[1008.54–1012.23]	[258–281]	6	6	[8.36–17.17]	6	[4.42–6.97]	6	[1.15–1.8]
Contreras	6	679	27.1	1	[1002.66–1014.47]	[235–280]	23	21	[0.79–2.47]	15	[1.4–28.02]	21	[0.95–7.3]
María Cristina	1	138	3.3	1	1004	245	2	2	[2.72–2.92]	2	[10.32–11.87]	2	0.75
Pedrera	1	111	12.7	1	1014.01	255	5	5	[0.86–1.19]	-	-	5	[2.95–3.25]
Regajo	3	407	0.8	1	[1009.43–1015.96]	[264–271]	10	10	[4.03–10.21]	10	[2.95–9.12]	10	[0.95–4.25]
Sitjar	2	584	3.2	1	[1015.56–1004]	[245–275]	4	4	[0.59–0.68]	4	[2.28–2.71]	4	[2.2–3.15]
Tous	4	163	9.8	1	[1007.74–1015.65]	[251–273]	9	9	[0.58–1.72]	6	[0.67–1.13]	9	[6–9.1]
Alfacs	2	0	56	35	[999.78–1011.34]	[243–249]	9	9	[3.65–6.73]	-	-	9	[1.55–3]
Pétrola	1	852	3.4	60	[1009.28–1015.07]	[239–267]	5	5	[77.58–309.2]	3	[142.27–162.33]	5	[0.17–0.45]
Total N	29	-	-	-	-	-	96	93	-	58	-	93	-

2.2. Field Radiometry

Water-leaving radiance was obtained by the measurement of the above-water radiometry taken within a three-hour interval before or after the satellite pass. An ASD FieldSpec® HandHeld2 spectroradiometer and an Ocean Optics (HR 4000) spectrometer were used (Table 2). The measurement procedure to obtain water-leaving radiance was carried out following the methodology described by Mobley, 1999 [15], with a zenith angle of 40° and an azimuth angle of 135° to minimize sun-glint perturbations. For each point, five measurements of the water-leaving radiance and total downward irradiance were taken using a reflectance panel made of Spectralon® (25% nominal reflectance). With this data, remote sensing reflectance (Rrs) of each measurement (Table 1) was obtained according to [15] and convolved to the S2-MSI spectral bands using the Sentinel-2 Spectral Response Functions (S2-SRF v2.0) [16].

Table 2. Spectroradiometer specifications.

Instrument	Ocean Optics HR4000	ASD FieldSpec® HandHeld 2
Manufacturer	Ocean Optics, Inc.; Orlando, FL, USA	Analytical Spectral Devices, Inc.; Boulder, CO, USA
Acceptance angle	8°	8°
Spectral sampling interval	0.2 nm	1 nm
Spectral range	200–1100 nm	325–1075 nm

2.3. Water Quality Measurements

Water quality parameters included Secchi disk depth (Z_{SD}), chlorophyll-a ([Chl-*a*]), and total suspended matter [TSM] concentrations. The Z_{SD} data were measured by submerging the Secchi disk vertically and slowly into the water until it was no longer visible. The Z_{SD} was then defined as the maximum visible Secchi disk depth. For [Chl-*a*] determination, water samples were filtered through 0.4–0.6 µm GF/F glass fiber filters, extracted using standard methods [17], and calculated with Jeffrey and Humphrey's (1975) equations [18]. The [TSM] was measured using the gravimetric method [19]. All water quality measurements were carried out coinciding with above-water radiometry measurements, but not all types of in situ measurements were available for all dates and locations (Table 1).

2.4. Sentinel-2 Data

The Sentinel-2 constellation consists of two satellites (S2A and S2B). Each one has onboard the MultiSpectral Instrument (S2-MSI). The S2-MSI TOA Level-1 (L1C) imagery includes information along 13 spectral bands centered at different wavelengths (~443–2200 nm) and with different spatial resolutions of 10, 20, and 60 m (Table 3). A set of 30 S2-MSI TOA (L1C) cloud-free images were downloaded from Copernicus Access Hub [20] coinciding with field radiometry measurements (Figure 2) and resampled to 20 m using the Graph Processing Tool (GPT) of the Sentinel Application Platform (SNAP v8.0) [21].

2.5. Atmospheric Correction Approaches

The Case 2 Regional Coast Colour is a development of the original Case 2 Regional processor [14], based on a multi-sensor per-pixel artificial neural network (NN) method [12]. It processes TOA images of a variety of sensors, including S2-MSI, and generates atmospherically corrected images. The output data include Rrs, as well as a set of automatic products for water quality such as [Chl-*a*] (conc_chla) and [TSM] (conc_tsm), and the depth of the water column from which 90% of the water-leaving irradiance is derived (Kd_z90max).

Table 3. S2A and S2B spectral bands, central wavelength (λ), spatial resolution, and application. Data from Copernicus Sentinel-2 MSI user guide [22]. The field 'C2-Nets' indicates the spectral bands outputted by C2-Nets (Y = yes, N = no).

Bands	ID in the Study	Spectral Region	Spatial Resolution (m)	λ_{S2A} (nm)	λ_{S2B} (nm)	Bandwidth $_{S2A–S2B}$ (nm)	C2-Nets
B1	B443	Coastal aerosol	60	442.7	442.2	21–21	Y
B2	B490	Blue	10	492.4	492.1	66–66	Y
B3	B560	Green	10	559.8	559	36–36	Y
B4	B665	Red	10	664.6	664.9	31–31	Y
B5	B705	Red-edge1	20	704.1	703.8	15–16	Y
B6	B740	Red-edge2	20	740.5	739.1	15–15	Y
B7	B783	Red-edge3	20	782.8	779.7	20–20	Y
B8	B842	NIR	10	832.8	832.9	106–106	N
B8A	B865	NIR narrow	20	864.7	864	21–22	Y
B9	B945	Water vapor	60	945.1	943.2	20–21	N
B10	B1620	SWIR/Cirrus	60	1373.5	1376.9	31–30	N
B11	B1620	SWIR1	20	1613.7	1610.4	91–94	N
B12	B2200	SWIR2	20	2202.4	2185.7	175–185	N

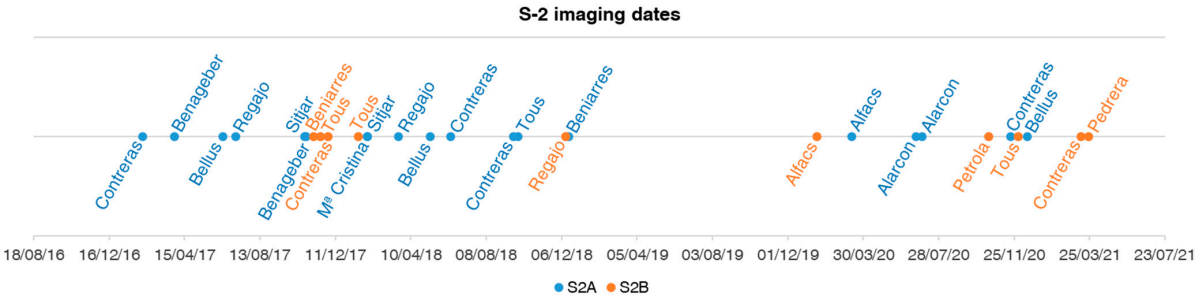

Figure 2. Temporal line of cloud-free S2 A/B images matching field measurements by study area.

The Case 2 Regional Coast Colour includes different processors (C2-Nets) which differ in the NN training ranges of inherent optical properties (IOPs; Table 4). The C2RCC-Net (here C2RCC) is the original net covering typical ranges of coastal IOPs. C2RCC was complemented with the CoastColour dataset to extend the range for coastal waters including extreme cases [23] resulting in the C2X-Net (C2X). The C2X-COMPLEX-Net (C2XC) was trained with intermediate ranges of IOPs, larger than C2RCC and tighter than C2X [24]. C2-Nets do not include specific correction for sun glint or land adjacency. The three C2-Nets were applied on all valid S2-MSI images (Figure 2) through the GPT of SNAP v8.0. The parametrization for the atmospheric correction of each image included: pressure (hPa) from NCEPR2 data [25] and O_3 (DU) from AuraOMI data [26] downloaded for each location and date from the ocean data archive of NASA [27]. Salinity (PSU) was estimated in each location by approximation with more frequent field measurements (Table 1). Despite the salinity of Pétrola being ~60 PSU (Table 1), it was set to 40 PSU, the maximum value accepted by the C2-Nets. Given the unavailability of water temperature measurements, it was left as default on all dates (15 °C). These site-specific parameters may influence atmospheric correction calculations introducing uncertainty in the estimation of the aerosol optical depth and are an inherent part in the C2-Nets NN processing [23]; thus, it is recommended to consider them for reducing estimation uncertainty. For land/water segmentation, the valid pixel expression was set as a threshold on the SWIR band B11 (Table 3) of S2-MSI L1C images. The threshold ranged between 0.025 and 0.11, and it was heuristically defined for each location and date according to the trade-off between keeping the maximum number of pixels of interest (water pixels inside study areas) and the minimum noise (e.g., mountain shadows, land). From each C2-Net, bands of TOA reflectance, remote sensing reflectance (Rrs), and Kd_z90max were extracted. The conc_chla and conc_tsm products

were also generated, with the default factors and exponents (conc_chla = 21 ∗ a_pig ^ 1.04; conc_tsm = 1.72 ∗ b_part + b_wit ∗ 3.1). In addition, C2-Nets flags [13], which include codes for quality control of pixels, were exported.

Table 4. IOP training ranges of the C2-Nets [23,24].

IOPs (m^{-1})	Description	C2RCC	C2X	C2XC
a_pig	Absorption coefficient of phytoplankton pigments	[≈0, 5.3]	[≈0, 51.0]	[≈0, 30.81]
a_det	Absorption coefficient of detritus	[≈0, 5.9]	[≈0, 60.0]	[≈0, 17.0]
a_gelb	Absorption coefficient of gelbstoff (CDOM absorption)	[≈0, 1.0]	[≈0, 60.0]	[≈0, 4.25]
b_wit	Scattering coefficient of white particles (calcareous sediments)	[≈0, 60.0]	[≈0, 590.0]	-
b_part	Scattering coefficient of typical sediments	[≈0, 60.0]	[≈0, 590.0]	-
b_tot	Scattering coefficient of typical sediment and white particles	-	-	[≈0, 1000.0]

2.6. Match-Up Exercise

The match-up exercise was performed for the three C2-Nets Rrs separately and applied to each validation dataset (i.e., in situ Rrs, [Chl-*a*], [TSM], and Z_{SD}).

(i) A 3 × 3 pixel window, centered at the coordinates of in situ measurements, was extracted for each date and location, and C2-Nets were quality-checked in all extracted pixels by applying the recommended flags [12]. These quality flags indicate issues related to the scope of the training range of the used NN and/or cloudy conditions [13,23] and should be considered for reducing potential artifacts and uncertainty.

(ii) Flagged pixels, as well as pixels with negative Rrs at bands B443, B490, B560, and B665 (Table 3), were removed from the analysis [28], and the number of remaining pixels within each pixel window was checked. Windows with fewer than 5 remaining pixels were removed from the analysis.

(iii) Outliers were defined through boxplot analysis applied separately to each pixel window and available spectral bands (B443-B783 and B865; Table 3).

(iv) Pixels with outliers in any of the bands were removed. The number of pixels within the pixel windows was revised once more, and those with fewer than 5 pixels remaining were removed from the analysis.

(v) The coefficient of variation (CV in Equation (1)) of B560 was computed for each remaining pixel window, removing those with CV > 15% [28].

$$CV = \sigma / \overline{x} * 100 \quad (1)$$

where σ is standard deviation and $\overline{x}$ is the mean.

2.7. Performance Assessment of C2-Nets

From the validation dataset to the analysis of the performance of the C2-Nets, the workflow is summarized in Figure 3.

2.7.1. Validation of Remote Sensing Reflectance (Rrs)

Validation of Rrs was broadly based on the scoring scheme proposed in [29]. However, match-up criteria and the number of statistics differed. In addition, all available C2-Nets spectral bands (Table 3) were included, validated, and used for the ranking in this study. The assessment was carried out with the maximum possible number of match-ups for each C2-Net.

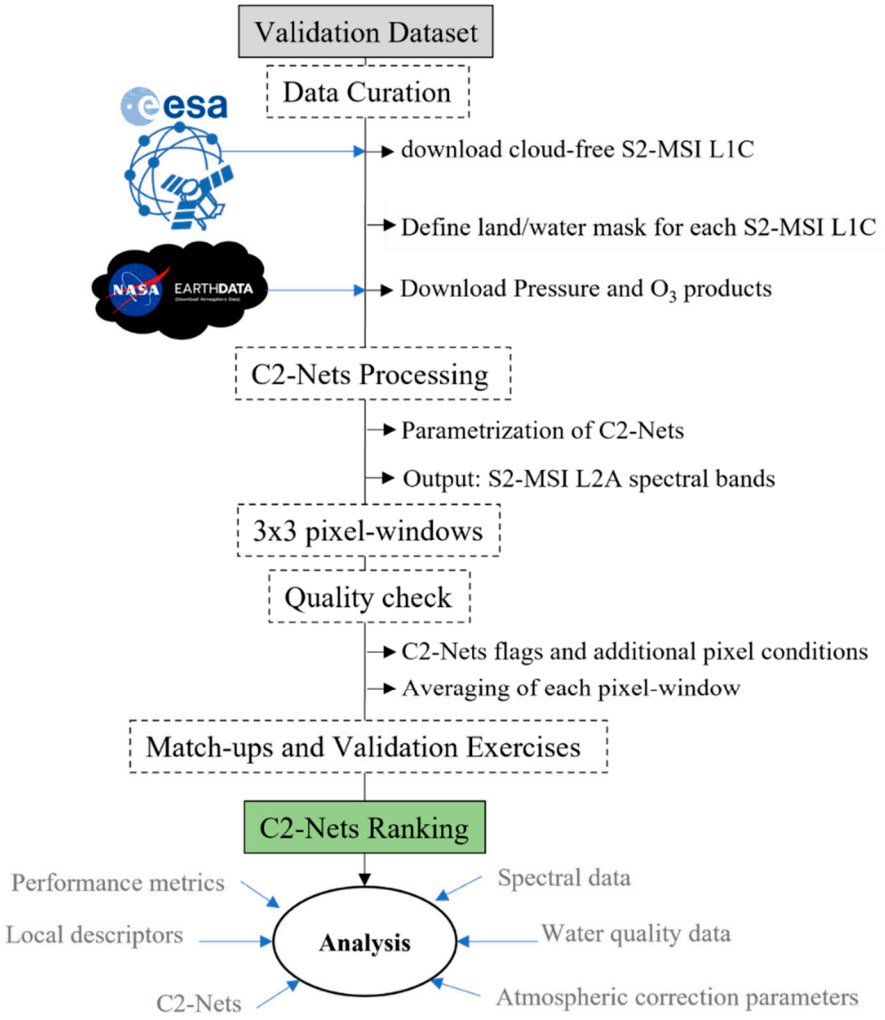

Figure 3. Workflow.

The scoring scheme extends the common validation strategy of comparisons between above-water measurements and satellite spectral bands by a ranking system.

(i) Bands scoring

For each C2-Net Rrs and TOA reflectance band, a set of 5 statistical parameters and their 95% confidence intervals were calculated for each available spectral band independently. The Root Mean Squared Error (*RMSE*), the Relative RMSE ($RMSE_{rel}$), the Bias, the RMSE of the Residual Error ($RMSE_{RE}$), and the Pearson's *r*, were computed and transformed into relative scores as in [29], evaluating the relationship of quality dependent on the C2-Net. For scoring purposes, Bias was used in absolute terms ($|Bias|$) and *r* was transformed to a negative orientated value (1–*r*). The *RMSE*, $RMSE_{rel,}$ and $RMSE_{RE}$ were used directly. To each property, the evaluation scores were assigned by band separately. The C2-Net with the smallest value in the statistical property received 2 points. Then, if a value corresponding to another C2-Net fell within the confidence interval of the best, this C2-Net received 2 points as well. If the value of a C2-Net was outside the confidence interval of the best but their confidence intervals overlapped, this algorithm received 1 point. Else, the C2-Net was given 0 points. See [29] for detailed information on the scoring-based method.

(ii) Spectral shape fitting

First, the spectral bias was removed by normalizing in situ and satellite-a-derived spectra to 560 nm (B560 in S2) before the evaluation. Chi-square tests (χ^2) of the in situ and C2-Nets-derived spectral shapes (including all available C2-Nets bands) were conducted for each match-up, and the percentage of chi-square values lower than the 95% confidence

level ($N\chi^2_{95}$) was calculated. Finally, the mean χ^2 ($\overline{\chi^2}$) for each C2-Net Rrs and TOA match-ups were derived.

(iii) Match-up efficiency

The relative number of valid match-ups (R_{matchs}) was calculated as the ratio between the valid observations after the match-up exercise for each C2-Net and the potential initial match-ups with in situ radiometry

2.7.2. Validation of Water Quality Products

In situ [Chl-*a*] and [TSM] were validated with the conc_chla and conc_tsm derived from C2-Nets with default factorization. The performance metrics selected for these parameters were the Mean Average Error (*MAE*; Equation (2)), the Root Mean Squared Error (*RMSE*; Equation (3)), the Bias (Equation (4)), and the Pearson's *r* (*r*). The kd_z90max is a variable strongly correlated with the Z_{SD} [30,31], however, being different variables, only the *r* was used for the comparison with the measured Z_{SD}. In addition, the coefficient of determination (R^2), the slope (*m*), and intercept (*b*) of linear regression were calculated.

$$MAE = \frac{1}{N}\sum_{i=1}^{N}|M_i - O_i| \quad (2)$$

$$RMSE = \sqrt{\sum_{i=1}^{N}\frac{(M_i - O_i)^2}{N}} \quad (3)$$

$$BIAS = \frac{1}{N}\sum_{i=1}^{N}(M_i - O_i) \quad (4)$$

where M_i are the estimated values from C2-Nets and O_i the field measured ones.

3. Results

3.1. In Situ Water Quality

The inclusion of different locations and dates involved wide ranges of water quality (Table 5). Most of the measurements corresponded to [Chl-*a*] < 3 mg/m^3 and [TSM] < 4 g/m^3 (median in Table 5). Minimum [Chl-*a*] and [TSM] (0.58 mg/m^3 and 0.74 g/m^3) were found in the Tous reservoir related with maximum Z_{SD} (9.1 m). Contrarily, maximum [Chl-*a*] and [TSM] (309.62 mg/m^3 and 162.33 g/m^3) were associated with the minimum Z_{SD} (0.17 m) in the hypertrophic salty lagoon of Pétrola.

Table 5. Number of water quality measurements by type (*N*), their concentration ranges (min, max), median, mean and standard deviation (σ).

WQ Parameters	*N*	*min*	*max*	*median*	*mean*	*σ*
[Chl-*a*] (mg/m^3)	93	0.58	309.6	2.72	20.55	61.5
Z_{SD} (m)	93	0.17	9.10	3.00	3.34	2.4
[TSM] (g/m^3)	58	0.67	162.3	3.65	13.70	33.5

3.2. Match-Up Analysis

The match-up exercise was carried out in a strict manner, thus maximizing the quality of the performance of each C2-Net. After the quality check, the number of match-ups was reduced by between ~12% to ~66% depending on the C2-Net and the type of in situ measurement (Figure 4). Most of the rejected match-ups were due to pixel windows having CV > 15% in B560. For all in situ datasets, a higher number of valid match-ups was found with C2RCC, while the lowest number was found for C2X (Figure 4).

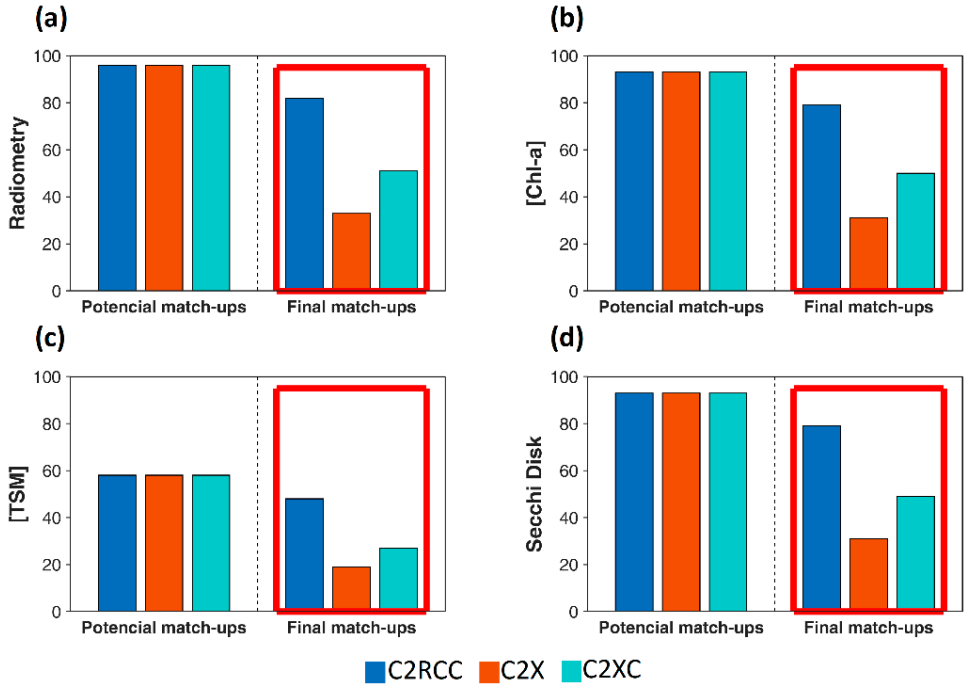

Figure 4. Match-up exercise by sub-dataset and C2-Nets: (**a**) Radiometry, (**b**) [Chl-*a*], (**c**) [TSM], (**d**) Secchi disk. Final match-ups for each C2-Net are highlighted with a red square.

3.3. Validation of Rrs

Comparing C2-Nets, disregarding the different number of match-ups, the bands' statistical results (Table A1) were translated into the similar scoring of C2RCC and C2XC in B443-B490, highest scoring of C2RCC in B560-B665, highest scoring of C2XC in B705-B783, and C2X ranking first in B865 (Figure 5a). Despite the winner's variability in single bands scoring, C2XC was the unique C2-Net scoring at all bands, ranking first in the total band score (Figure 5b). C2X did not score in B665 and C2RCC and did not achieve any point from B740-B865 (Figure 5a).

In general terms, all C2-Nets tended to underestimate Rrs of blue and green bands, with most of the errors within the [−50, 50] % interval (Figure 6). Relative errors were more dispersed between B665-B865 and C2XC, and C2X clearly improved C2RCC in cases with greater NIR Rrs (Figure 6). These led to better fitting of C2X and C2XC Rrs in NIR wavelengths (Figure A1) and contributed to making C2XC (which included higher relative number of match-ups with greater NIR Rrs) the most capable of retaining the spectral shape with $\overline{\chi^2}$ closest, to 0 ($\overline{\chi^2} = -0.02$) and maximum $N\chi^2 = 1$ (Figure 5b).

However, with C2RCC more radiometry match-ups (85%) were kept than with C2XC (53%) and C2X (33%). Match-ups with high reflectance pixels with peaks in B560 and B705 and/or greater NIR Rrs were more susceptible to rejection with C2RCC (e.g., Pétrola in Figure A2g), and potential match-ups related to more clear waters with lower Rrs along the spectrum and/or a single peak in B560 were more likely rejected with C2X and C2XC (e.g., Tous in Figure A2f). This was visible even from TOA reflectance (Figure 7), although all C2-Nets included match-ups with different types of spectrums (e.g., Figure A2a,c).

Exploring the relation of the performance of C2-Nets with TOA reflectance, a k-means classification (4 classes) was conducted including TOA reflectance, in situ Rrs, and C2-Nets Rrs separately for C2-Nets (Figure 8). Clusters found for different C2-Nets were grouped by similarity (proximity) in cluster centers. In general terms, the clusters C1 and C4 (Figure 8) grouped those pixels with TOA and C2-Nets peaks at 560 and 705 nm, frequently associated with increasing NIR Rrs (e.g., Figure A2b,d,e). Clusters C* and C** fit in the same category, although the small numbers of match-ups (Figure 8a) mainly highlight the

trends of four locations and dates which were included in C1 or C4 with the C2RCC dataset (e.g., Figure A2c) or only accepted with C2XC (Figure A2g).

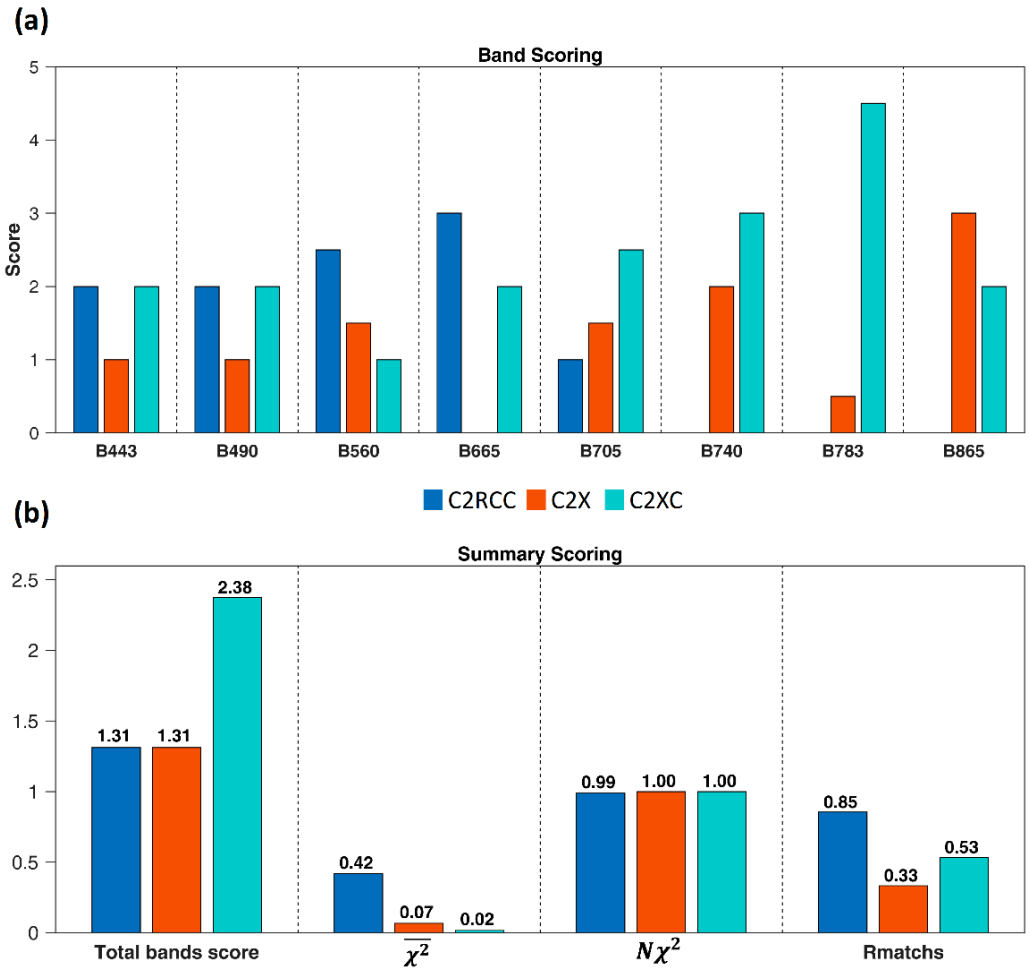

Figure 5. (**a**) Band scoring per C2-Nets Rrs. (**b**) Summary of the validation of Rrs. For representation, $\overline{\chi^2}$ is presented in absolute values, and all band scores were summed and divided by the number of available bands (N_{bands} = 8) to compute the total band score.

The C3 class grouped more than 50% of the valid match-ups of the three C2-Nets (Figure 8a), including smoother TOA reflectance spectrums generally related to lower NIR Rrs and/or presence of a single/dominant C2-Nets B560 peak (e.g., Figure A2f,h). The match-ups of the C2 class were only included with C2RCC and C2XC (Figure 8), and all of them correspond to the same location and date. These spectrums were characterized by high TOA reflectance in all spectral regions (Figure 8a), including relatively high SWIR reflectance (Figure A2d), although the in situ Rrs was similar to the measurements in C3 (Figure 8b).

3.4. Validation of Water Quality

For [TSM] and [Chl-*a*], the *MAE*, *RMSE*, *Bias*, and Pearson's *r* analysis were conducted. For assessing the Kd_z90max and Z_{SD} relationship, only Pearson's *r* was calculated. Both for [TSM] and [Chl-*a*], C2RCC achieved the lowest *MAE* and *RMSE*, with *BIAS* closest to 0, followed by C2X and C2XC (Table 6). However, the C2XC dataset included extreme measured [Chl-*a*] and [TSM] (Table 6), for which high underestimation was observed (Figure 9a,b). Such extreme match-ups had a high impact on C2XC-derived *MAE*, *RMSE*, and *Bias* (Table 6), but higher relationships between measured and derived [Chl-*a*] (r = 0.94) and [TSM] (r = 0.81) from the C2XC dataset were observed (Table 6). Despite this, relative

errors were highly variable even for [Chl-*a*] < 25 mg/m^3 and [TSM] < 25 g/m^3, leading to uncertain retrievals, especially for [Chl-*a*].

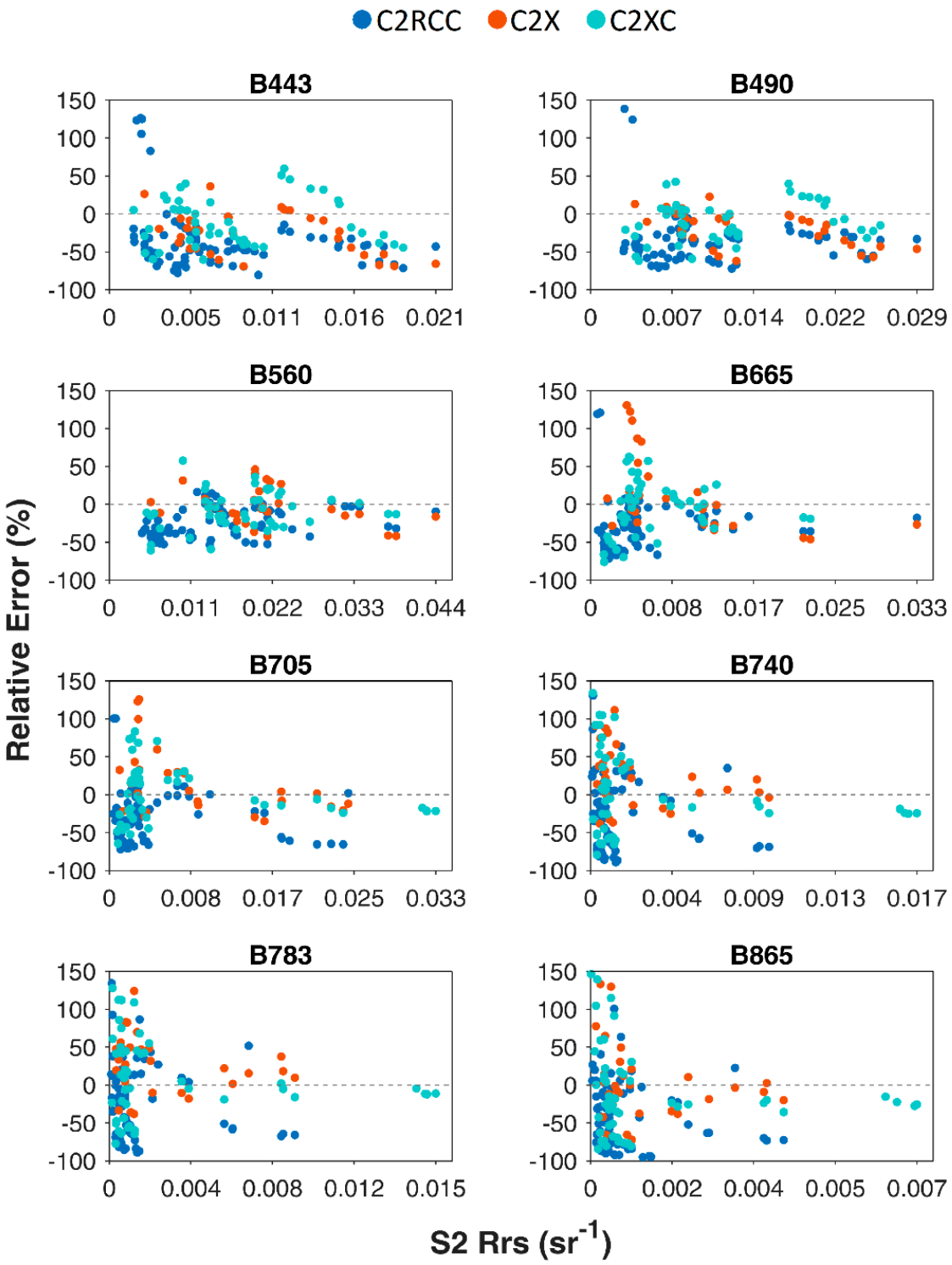

Figure 6. The relative error between measured and C2-Nets-derived Rrs at all available spectral bands for each C2-Net. Relative error was computed for representation as [(measured Rrs–C2-Nets Rrs)/measured Rrs ∗ 100].

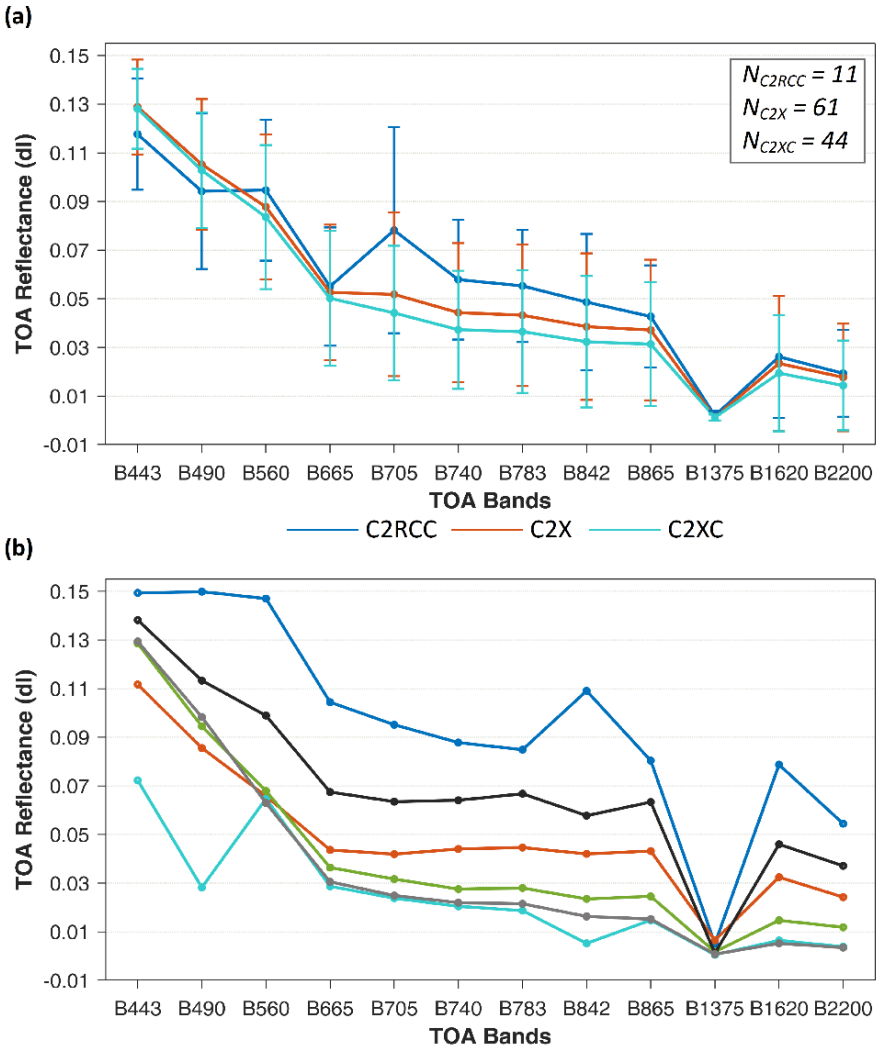

Figure 7. (**a**) Mean (lines) and standard deviation (bars) of TOA reflectance spectrums describing, by C2-Net, the set of rejected pixels during the match-up exercise steps ii–v; (**b**) Mean TOA spectrums of rejected pixels in all C2-Nets. Rejected pixels of the C2-Nets flags are not included.

Table 6. Summary of validation of [Chl-*a*], [TSM], and Kd_z90max derived from C2-Nets. *m* and *b* stand for slope and intercept of the linear regression.

C2Net	Parameter	In Situ *min–max*	C2-Nets *min–max*	*MAE*	*RMSE*	*Bias*	*r*	R^2	*m*	*b*
C2RCC	[Chl-*a*]	0.58–68.01	0.43–23.68	5.7	11.5	−1.16	0.72	0.52	0.26	4.38
C2X		0.61–68.01	1.84–100.25	10.2	17.3	5.85	0.81	0.66	1.16	3.96
C2XC		0.59–309.20	0.01–139.56	17.8	48.1	−12.1	0.94	0.88	0.45	5.03
C2RCC	[TSM]	0.74–28.02	0.93–19.13	2.9	4.6	−0.13	0.75	0.56	0.65	2.17
C2X		2.28–28.02	3.84–56.22	10.9	14.9	8.77	0.68	0.46	1.42	3.95
C2XC		2.28–162.33	0.33–58.52	13.1	29.0	−2.76	0.81	0.65	0.33	9.71
C2RCC	Z_{SD}	0.45–9.1	0.45–7.03	-	-	-	0.77	0.59	1.09	0.08
C2X		0.45–5.80	0.27–4.00	-	-	-	0.82	0.67	1.09	0.29
C2XC		0.17–7.70	0.27–6.63	-	-	-	0.94	0.88	0.88	0.12

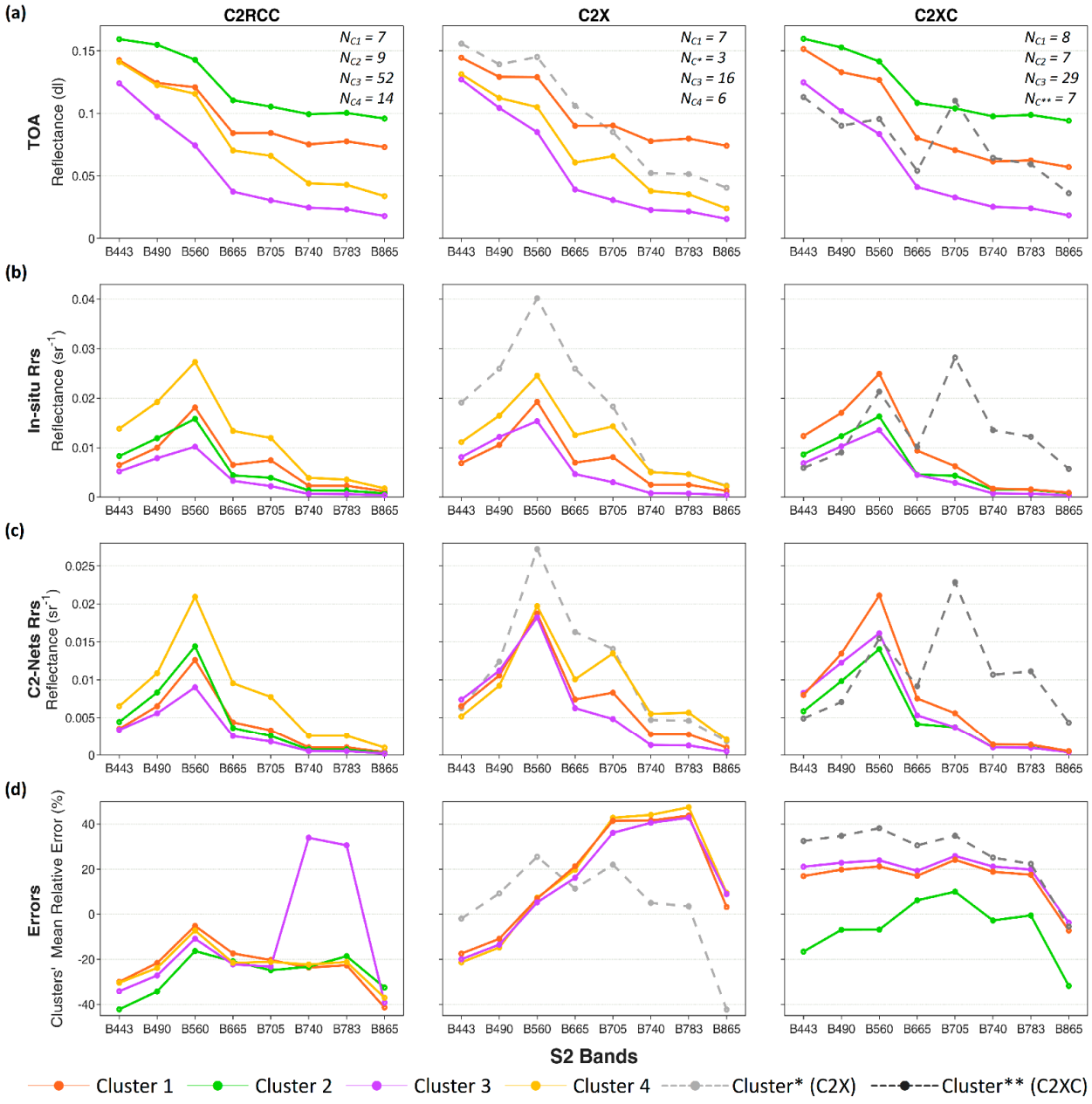

Figure 8. K-means clustering including TOA reflectance and measured and C2-Nets-derived Rrs (**a**–**c**). Lines represent, by C2-Net (columns), cluster centers for (**a**) TOA reflectance, (**b**) in situ Rrs, (**c**) C2-Nets Rrs, and (**d**) mean relative error of cluster members' in situ and C2-Nets Rrs. For ease of representation, clusters are colored according to the similarity between C2-Nets classes.

Regarding Z_{SD}, the highest correlation was observed with Kd_z90max derived from C2XC (r = 0.94), but r > 0.75 was retrieved with all C2-Nets (Table 6). The Kd_z90max from C2RCC included a subset of the in situ Z_{SD} measurements corresponding to increasingly clear waters with Z_{SD} > 6 m (match-ups mainly included by C2RCC). The Kd_z90max was lower than Z_{SD} for this set of points (Figure 9c).

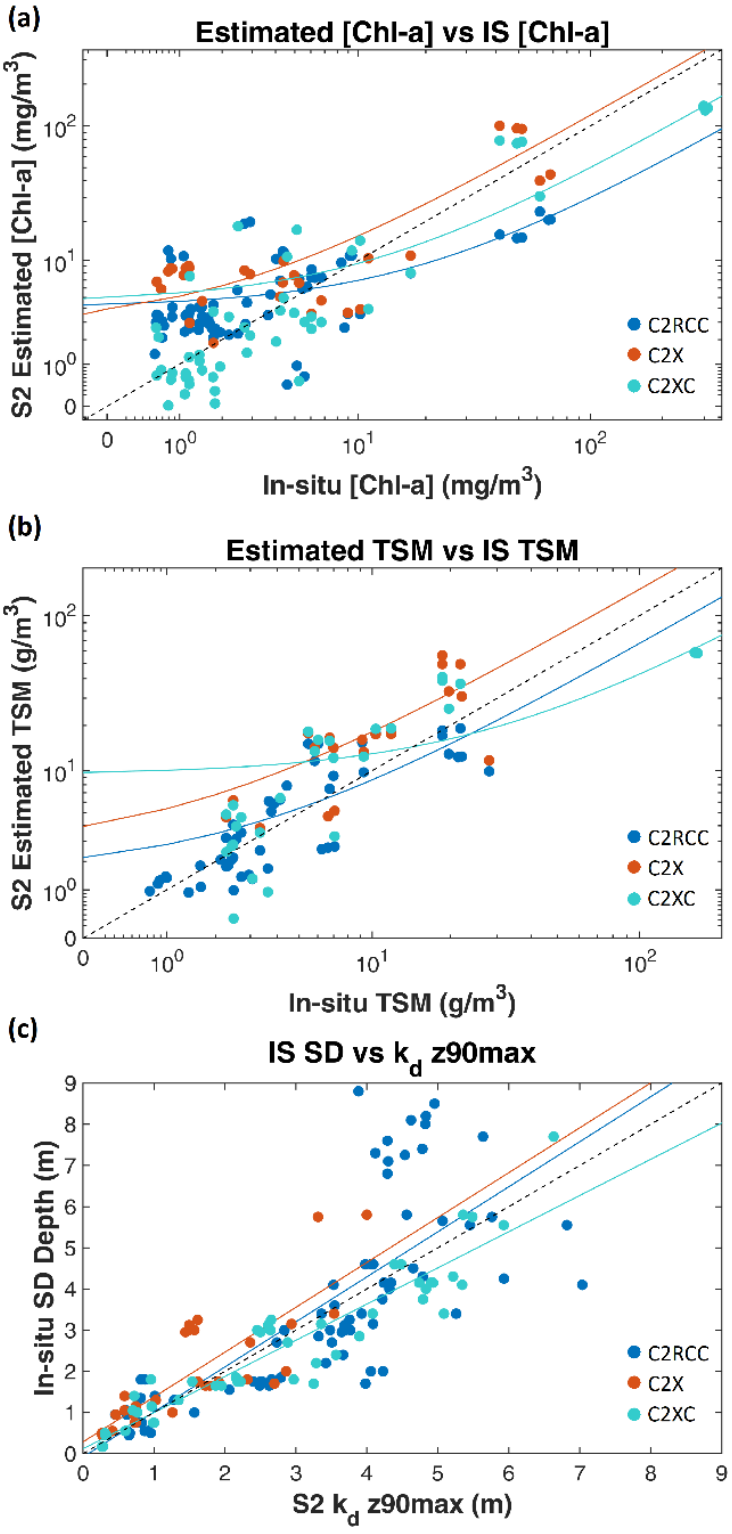

Figure 9. Scatter plots of in situ and C2-Nets estimated (**a**) [Chl-*a*], (**b**) [TSM], and (**c**) Z_{SD}. Plots in (**a**) and (**b**) are shown in logarithmic scale for ease of interpretation. The dashed line corresponds to a 1:1 line.

4. Discussion

To date, only C2RCC and C2X have been previously explored for retrieval of water surface reflectance or water quality (e.g., [12,32]). This study evaluates the new C2XC processor, comparing it to the previous C2RCC and C2X.

4.1. Performance on Retrieval of Rrs with C2-Nets

Comparing C2-Nets scoring (Figure 5), C2X and C2XC retained the spectral shape better than C2RCC, with C2XC outperforming C2X in all bands except B560 and B865 (Figure 5a) and showing greater consistency than other C2-Nets in the relative errors of B443-B783 through different types of waters (Figure 8d). However, with C2X and C2XC, a great number of pixel windows were rejected (Figure 4), mainly related to oligotrophic–mesotrophic waters. Most of these match-ups were only kept with C2RCC. Contrarily, the match-ups rejected with C2RCC were related to higher Rrs and associated with green (B560) and NIR (B705) peaks (C1 and C2 in Figure 8). In these scenarios, C2RCC tended to highly underestimate Rrs, even overlooking spectral peaks, limiting the use of this processor in eutrophic–hypertrophic waters. In those scenarios, C2X and C2XC retrieved the peaks more accurately, especially in the NIR (e.g., Figure A2c,e), although they tended to mismatch in the green peaks, especially in the presence of large B705 reflectance (e.g., Figure A2b,e,g). This may be related to the absorption of colored dissolved organic matter (CDOM), as found in [33] in lakes with high concentrations of optically active constituents, where CDOM absorbs most of the light in the blue part of the spectrum [34], complicating the optimum retrieval of IOPs and leading to mismatching of peaks in green bands. Even so, C2X and C2XC provided for a better representation of the overall spectral shape in more turbid waters.

The different performances of C2-Nets along different scenarios could be explained by the different range of training datasets (Table 4) and the minimization of adverse effects by the NN [35]. The C2RCC showed better performance in oligotrophic–mesotrophic waters, but in ultraoligotrophic waters (clear waters with Z_{SD} > 3 m and [Chl-*a*] < 2.5 mg/m^3) accurate retrieval of Rrs was complicated (e.g., Figure A2f) as also observed in [13]. The C2XC was suitable for more complex waters (up to hypereutrophic reservoirs) but also improved the performance of C2RCC in some mesotrophic scenarios, such as coastal waters in Figure A2h. Although C2X has been observed to be more suitable for coastal and complex waters than for clear waters [13,32,35], the reduced number of valid match-ups (33%) and lower consistency in the accuracy along the spectrum observed with this processor made it the most uncertain C2-Net. This could be related to the large training range of IOPs of C2X, which may allow good Rrs retrievals to be achieved in different types of scenarios (e.g., Figure A2b,e)—including oligotrophic–clear and eutrophic–turbid lakes [36]—although the width of IOP ranges may also introduce a risk of diverging from the actual solution from the inversion, leading to confusion [33].

4.2. Recommendation on the Selection of C2-Nets

The aforementioned suggests combining C2-Nets to improve Rrs estimates in a wide range of scenarios. The choice of the C2-Nets could be limited to C2RCC and C2XC for most of the scenarios observed in the studied areas targeted. Different studies have proposed to switch between atmospheric correction methods depending on optical water types (OWTs). To define OWT, [37] developed a classification based on key features of the Rrs reflectance spectrum, such as the location of the spectral maximum, slopes, and amplitude. However, the choice of the atmospheric correction processor strongly affects the OWT classification and has to be performed after the atmospheric correction process. In [13], it was observed that the accuracy of several atmosphere correction processors improved markedly after the prior classification of water types defined by [Chl-*a*] and Z_{SD} ranges of in situ measurements. However, this kind of classification implies prior knowledge on dynamic ranges of water quality parameters, and biophysical characteristics are not always the unique factor defining the performance of C2-Nets (see Figure A2a,b).

To improve these approaches, we suggest that research focused on the classification of TOA optical types might be useful for selecting the optimum C2-Net, improving accuracy in the retrieval of Rrs. The TOA measurements do not require prior knowledge of the conditions of the studied area and somehow include information on the atmosphere, the optical properties of water, and additional effects such as sun glint or land adjacency. A simplistic classification of the TOA reflectance spectrum and its relationship with C2-Nets choice is shown (Figure 8). Further research including more data and deeper classification analysis should also be conducted attending to the severity of sun glint and the effect of land-adjacency, which have a larger impact in small inland waters [38]. After selection and processing with the optimum C2-Net, methods accounting for spectral shape, magnitude, and distinctive Rrs spectral features (e.g., [37,39,40]) will be further evaluated for accurately defining the OWT.

4.3. Recommendations for Water Quality Estimation with C2-Nets

For estimation of Z_{SD}, the Kd_z90max band derived from C2-Nets showed great potential (Figure 6), particularly with C2XC (Table 6). Despite this, estimating the ZSD in clear waters seems more challenging, while in other meso-eutrophic waters, light attenuation-related products have already demonstrated great accuracy [36]. Other studies proposed to use the B560/B705 ratio [41] for estimating Z_{SD}, but this approach should be more limited to mesotrophic–eutrophic waters since in hypereutrophic waters accuracy in green reflectance decreases, which may lead to higher uncertainty of this band ratio in turbid waters. Regarding [Chl-*a*] and [TSM], both conc_chla and conc_tsm bands from C2-Nets did not provide acceptable estimations, and their use with default parameters (factors and exponents) is not suitable for the whole range of optically active constituent concentrations and scenarios targeted here. The performance of C2-Nets' [Chl-*a*] and especially [TSM] products could be improved by recalibrating with in situ data the factors used in the C2-Nets for their computation, but they might need to be adapted for specific locations. A common alternative approach is to switch between different empirical and bio-optical algorithms depending on the optical water type (OWT). Algorithm blending based on OWT has proven to be superior to single algorithms when considering the entire dynamic range of environmental conditions [40].

In general terms, for estimation of [Chl-*a*] in more complex waters, it would be recommended to avoid the use of blue and green bands, with higher uncertainty in the presence of peaks in B705. Also, in eutrophic waters, the reflectance peak of phytoplankton shifts towards longer wavelengths, and the use of B705 is recommended [5,42,43]. Thus, in those cases, the combined use of red and NIR bands—for which C2XC and C2X showed better agreement with in situ Rrs in these types of waters—must be considered. For instance, band ratios based on red–NIR combinations have been demonstrated to be able to accurately retrieve [Chl-*a*] in turbid eutrophic waters [42,44,45]. In more clear waters, related to oligo-mesotrophic status, empirical standard algorithms based on VIS combinations such as OC2, OC3, and OC4 are frequently applied with an accurate estimation of [Chl-*a*] [13,40,42]. The use of blue and green bands is appropriated in oligotrophic waters (<4 mg/m^3), although red bands contain relevant information for retrieving [Chl-*a*] in these types of waters too [32], and the retrieval of [Chl-*a*] through the combination of red and green bands has shown less sensitivity to the atmospheric correction in oligotrophic to mesotrophic waters [6].

For the estimation of [TSM], the optimal spectral range is located between 680 and 730 nm [46], and different studies propose to exploit the B705 band, alone or in combination with VIS bands, with which linear relationships have been observed for a wide range of TSM concentrations [41,47,48].

5. Conclusions

The study highlights the potential of the combination of C2-Nets processors for improving the accuracy and consistency of water surface reflectance estimates on a pixel-wise basis. Within the processors, this study is one of the first attempts to test the capabil-

ities of C2XC, the most recent evolution of the C2RCC. The results suggest that combining the use of C2RCC and C2XC—depending on the pixel optical type in the TOA—would lead to improved accuracy in the retrieval of Rrs in a wide range of waters, along with several different scenarios. Regarding the retrieval of water quality parameters, the C2-Nets Kd_z90max product demonstrated great capabilities as a proxy of Z_{SD}. However, for estimating [Chl-*a*] and [TSM], the use of the products included in the output of the C2-Nets, with default factors and exponents, is limited and site-specific. Thus, different approaches might be selected, including the recalibration of the constants in the C2-Nets parametrization or the blending of different algorithms, depending on the optical water type and the related performance of the atmospheric correction. An in-depth exploration of TOA reflectance classification could contribute to an accurate selection and combination of C2-Nets and their further evolution, which suggests a promising future for supporting the monitoring of inland and coastal waters.

Author Contributions: Conceptualization, J.S.-G., E.P.U., E.A. and J.D.; methodology, J.S.-G., E.P.U., E.A., C.A. and C.T.; formal analysis, J.S.-G., E.P.U., C.A. and A.R.-V.; data curation, J.S.-G., E.P.U., C.T. and X.S.-P.; writing—original draft preparation, J.S.-G. and E.P.U.; writing—review and editing, J.D., A.R.-V., C.T., X.S.-P., E.A., E.V. and C.A.; supervision, J.M.; funding acquisition, J.M. All authors have read and agreed to the published version of the manuscript.

Funding: Jesús Soriano held a pre-doctoral grant funded by Agència de Gestió d'Ajuts Universitaris i de Recerca (2020FI_B2 00148). Esther Patricia Urrego holds a pre-doctoral grant funded by Ministerio de Ciencia, Innovación y Universidades (PRE2019-088232). This research was partially funded by the European Union—ERDF and the Ministry of Science and Innovation and the State Research Agency of Spain under project RTI2018-098651-B-C51 (FLEXL3L4—Advanced Products L3 and L4 for the FLEX-S3 mission).

Institutional Review Board Statement: Not applicable.

Informed Consent Statement: Not applicable.

Data Availability Statement: The data presented in this study are available on request from the corresponding author.

Acknowledgments: The authors especially acknowledge the work of the team of researchers and technicians of the Institut d'Investigació i Tecnologia Agroalimentàries (IRTA) that participated in the field surveys and laboratory analysis.

Conflicts of Interest: The authors declare no conflict of interest. The funders had no role in the design of the study; in the collection, analyses, or interpretation of data; in the writing of the manuscript; or in the decision to publish the results.

Appendix A

Table A1. Band statistics for TOA and Rrs derived from C2-Nets datasets. Best results for each band and statistic are highlighted.

C2Net	Band	*RMSE*	$RMSE_{rel}$	$RMSE_{RE}$	$\lvert Bias \rvert$	*r*
C2RCC_TOA	B443	0.1260	30.900	0.0139	0.1250	0.615
C2RCC_Rrs		0.0043	0.548	0.0030	0.0031	0.817
C2X_TOA		0.1250	20.200	0.0109	0.1240	0.672
C2X_Rrs		0.0052	0.4970	0.0044	0.0029	0.568
C2XC_TOA		0.1250	28.200	0.0159	0.1240	0.682
C2XC_Rrs		0.0036	0.806	0.0035	0.0004	0.739
C2RCC_TOA	B490	0.1020	14.850	0.0193	0.0997	0.639
C2RCC_Rrs		0.0051	0.552	0.0036	0.0036	0.853
C2X_TOA		0.1010	10.300	0.0140	0.0998	0.717
C2X_Rrs		0.0059	0.476	0.0049	0.0033	0.728
C2XC_TOA		0.1030	14.100	0.0207	0.1006	0.642
C2XC_Rrs		0.0041	0.886	0.0041	0.0000	0.814

Table A1. *Cont.*

C2Net	Band	$RMSE$	$RMSE_{rel}$	$RMSE_{RE}$	$\lvert Bias \rvert$	r
C2RCC_TOA	B560	0.0819	8.490	0.0235	0.0785	0.740
C2RCC_Rrs		0.0047	0.587	0.0040	0.0025	0.894
C2X_TOA		0.0849	5.720	0.0189	0.0828	0.794
C2X_Rrs		0.0062	0.517	0.0061	0.0010	0.747
C2XC_TOA		0.0861	8.290	0.0226	0.0831	0.635
C2XC_Rrs		0.0051	0.921	0.0050	0.0003	0.809
C2RCC_TOA	B665	0.0557	20.720	0.0252	0.0496	0.517
C2RCC_Rrs		0.0022	0.543	0.0017	0.0014	0.972
C2X_TOA		0.0551	11.080	0.0212	0.0509	0.720
C2X_Rrs		0.0039	0.600	0.0038	0.0006	0.863
C2XC_TOA		0.0579	20.600	0.0251	0.0522	0.332
C2XC_Rrs		0.0018	0.710	0.0018	0.0000	0.921
C2RCC_TOA	B705	0.0519	29.300	0.0262	0.0449	0.581
C2RCC_Rrs		0.0036	0.560	0.0033	0.0015	0.845
C2X_TOA		0.0524	14.226	0.0237	0.0467	0.798
C2X_Rrs		0.0026	0.793	0.0026	0.0004	0.949
C2XC_TOA		0.0593	29.300	0.0283	0.0520	0.690
C2XC_Rrs		0.0024	0.753	0.0024	0.0004	0.985
C2RCC_TOA	B740	0.0467	78.200	0.0257	0.0391	0.282
C2RCC_Rrs		0.0014	4.690	0.0014	0.0005	0.741
C2X_TOA		0.0422	42.000	0.0209	0.0367	0.476
C2X_Rrs		0.0007	0.761	0.0006	0.0004	0.975
C2XC_TOA		0.0508	86.300	0.0263	0.0435	0.347
C2XC_Rrs		0.0013	0.673	0.0012	0.0004	0.990
C2RCC_TOA	B783	0.0468	65.640	0.0268	0.0384	0.281
C2RCC_Rrs		0.0014	4.332	0.0013	0.0004	0.728
C2X_TOA		0.0423	40.990	0.0222	0.0361	0.460
C2X_Rrs		0.0009	0.753	0.0007	0.0005	0.977
C2XC_TOA		0.0506	84.802	0.0272	0.0427	0.289
C2XC_Rrs		0.0007	0.576	0.0007	0.0001	0.996
C2RCC_TOA	B865	0.0430	246.000	0.0274	0.0332	0.194
C2RCC_Rrs		0.0007	0.635	0.0006	0.0004	0.694
C2X_TOA		0.0371	55.900	0.0224	0.0296	0.313
C2X_Rrs		0.0004	0.659	0.0003	0.0001	0.957
C2XC_TOA		0.0455	291.000	0.0277	0.0361	0.077
C2XC_Rrs		0.0006	0.591	0.0005	0.0003	0.985

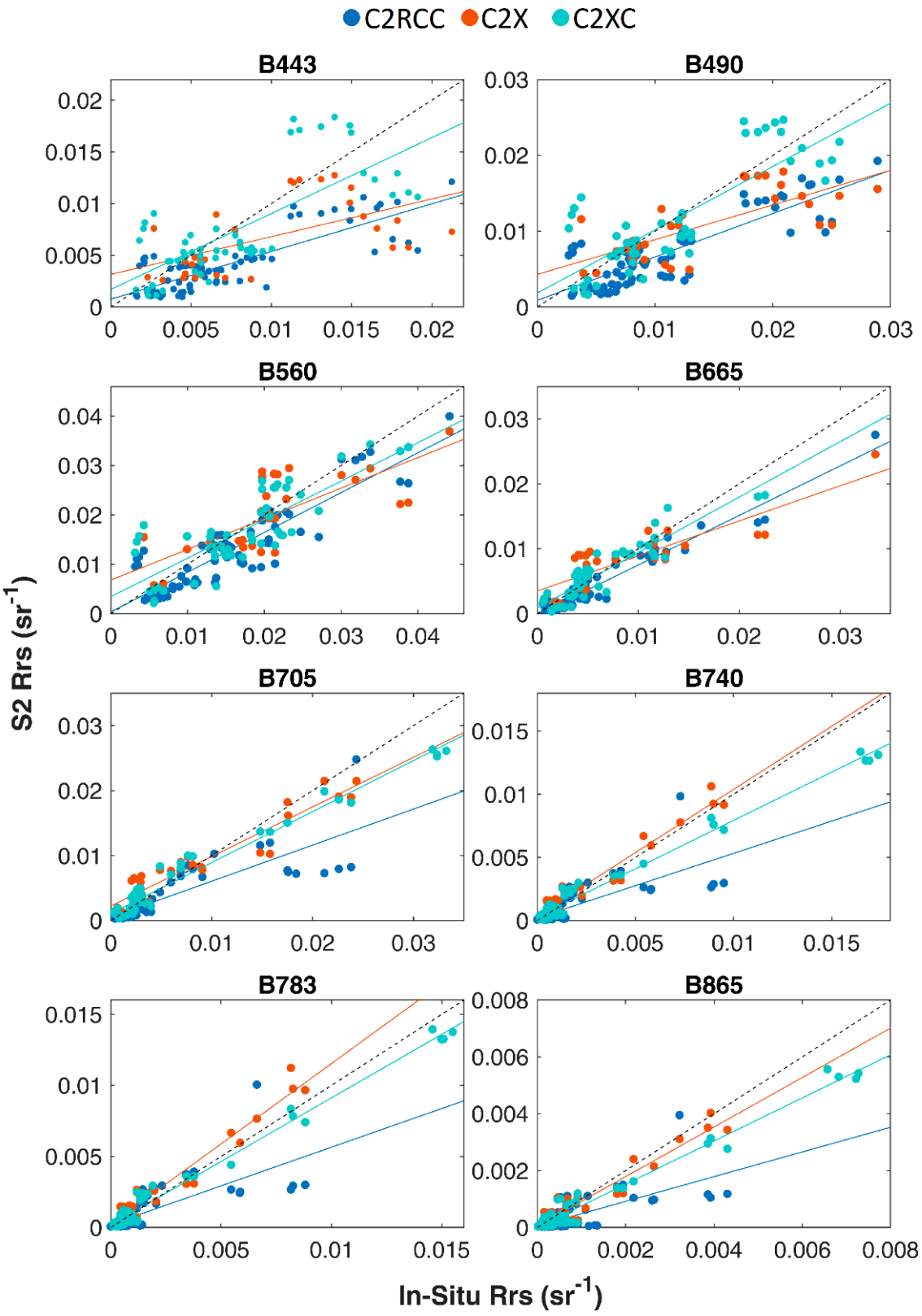

Figure A1. Scatter plots between measured and C2-Nets estimated Rrs at all available spectral bands. The dashed line corresponds to a 1:1 line.

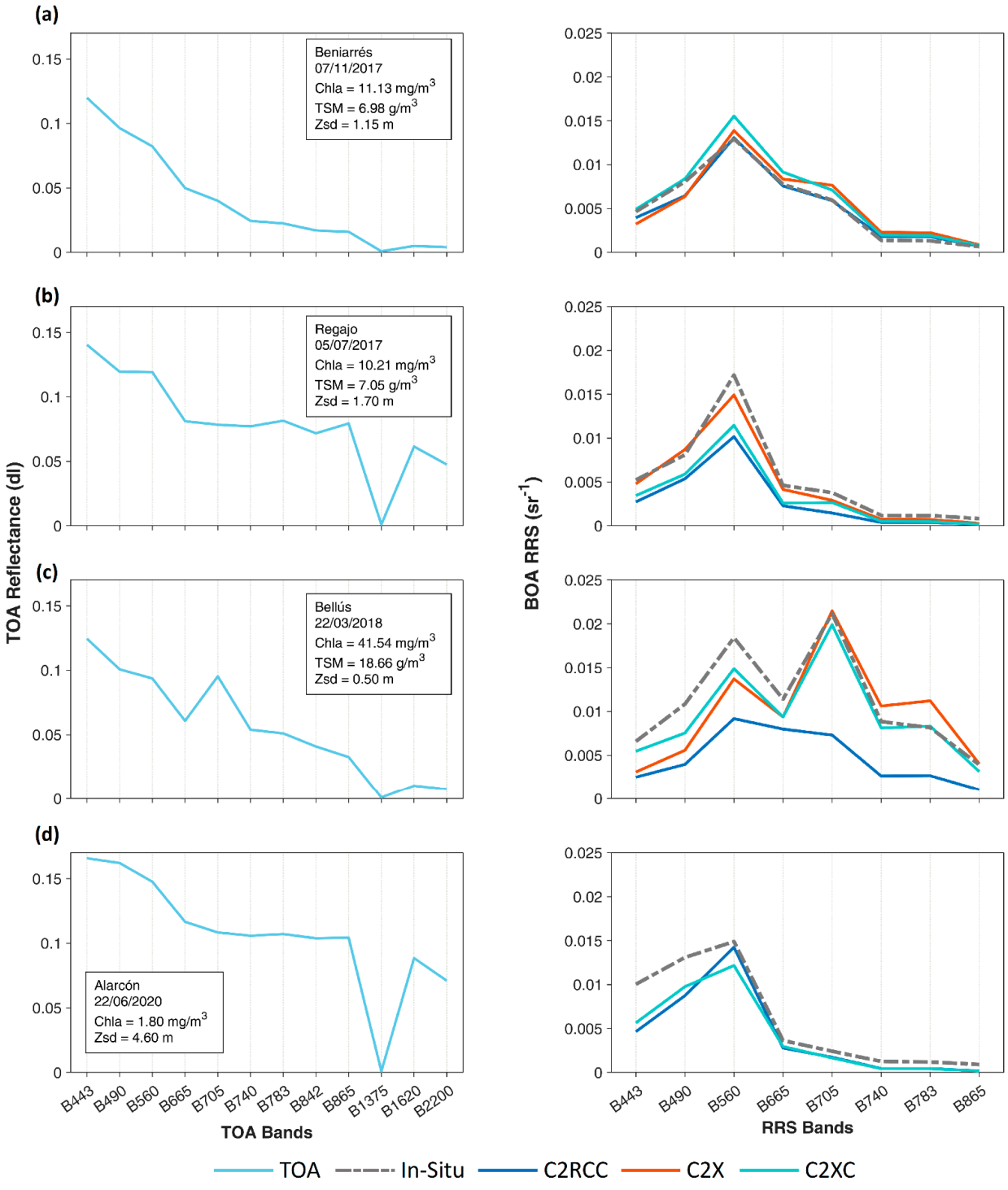

Figure A2. *Cont.*

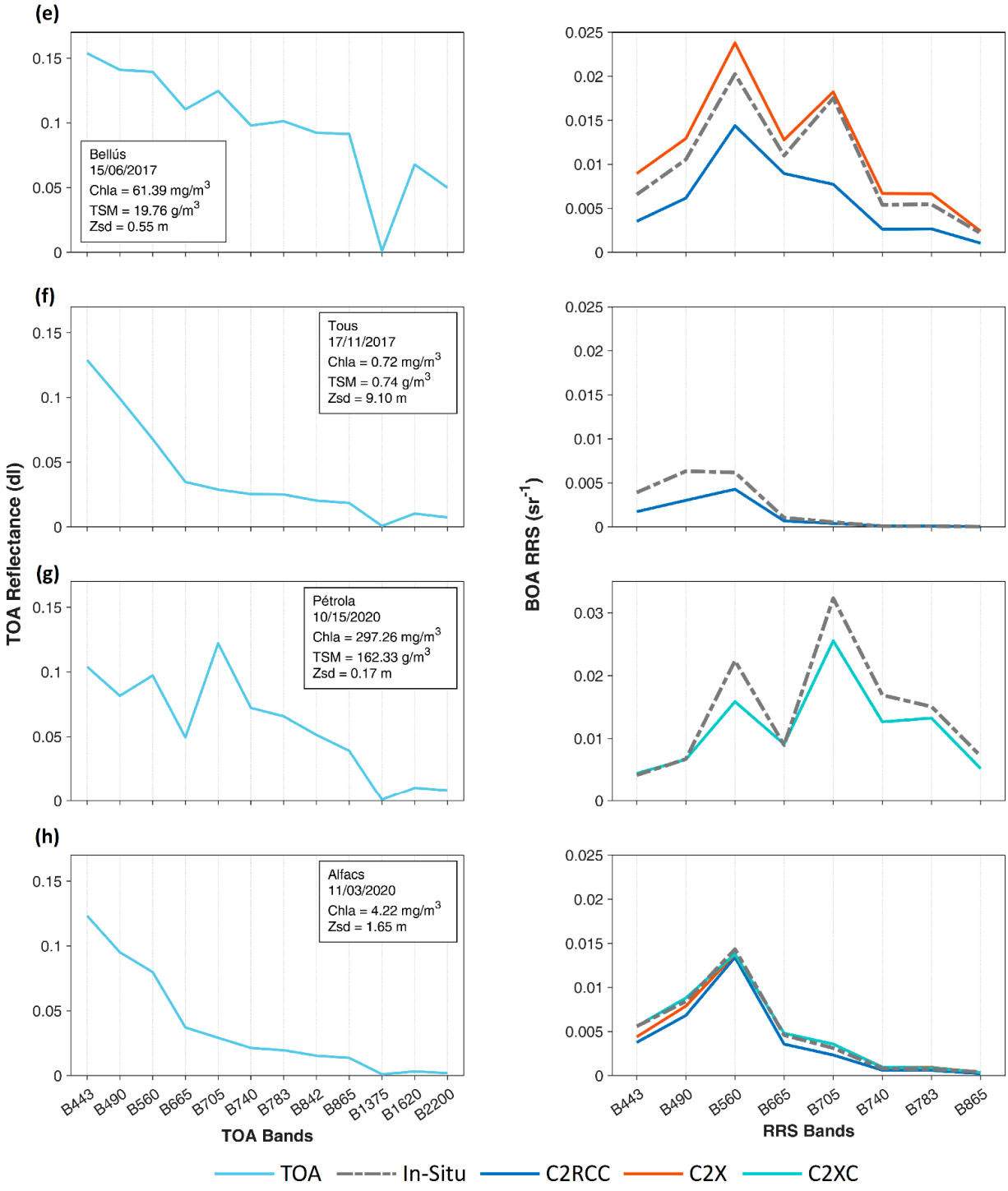

Figure A2. TOA reflectance spectrums (left column) and in situ and C2-Nets estimated Rrs (right column) for different scenarios (**a**–**h**). Availability of C2-Nets Rrs depends on the pixel flagging criteria described in the paper.

References

1. Dörnhöfer, K.; Klinger, P.; Heege, T.; Oppelt, N. Multi-sensor satellite and in situ monitoring of phytoplankton development in a eutrophic-mesotrophic lake. *Sci. Total Environ.* **2018**, *612*, 1200–1214. [CrossRef] [PubMed]
2. Kutser, T.; Paavel, B.; Verpoorter, C.; Ligi, M.; Soomets, T.; Toming, K.; Casal, G. Remote sensing of black lakes and using 810 nm reflectance peak for retrieving water quality parameters of optically complex waters. *Remote Sens.* **2016**, *8*, 497. [CrossRef]
3. Mostert, E. The European Water Framework Directive and water management research. *Phys. Chem. Earth A/B/C* **2003**, *28*, 523–527. [CrossRef]
4. Gholizadeh, M.; Melesse, A.; Reddi, L. A Comprehensive Review on Water Quality Parameters Estimation Using Remote Sensing Techniques. *Sensors* **2016**, *16*, 1298. [CrossRef]
5. Toming, K.; Kutser, T.; Laas, A.; Sepp, M.; Paavel, B.; Nõges, T. First experiences in mapping lake water quality parameters with sentinel-2 MSI imagery. *Remote Sens.* **2016**, *8*, 640. [CrossRef]
6. Soriano-González, J.; Angelats, E.; Fernández-Tejedor, M.; Diogene, J.; Alcaraz, C. First Results of Phytoplankton Spatial Dynamics in Two NW-Mediterranean Bays from Chlorophyll-a Estimates Using Sentinel 2: Potential Implications for Aquaculture. *Remote Sens.* **2019**, *11*, 1756. [CrossRef]
7. Bakker, W.H.; Gorte, B.G.H.; Horn, J.A.; Janssen, L.L.F.; Pohl, C.; Parkash, A.; Reeves, C.V.; Weir, M.J.C.; Woldai, T. *Principles of Remote Sensing: An Introductory Textbook*; ITC Educational Textbook Series 2; The International Institute for Aerospace Survey and Earth Sciences (ITC): Enschede, The Netherlands, 2001.
8. IOCCG. *Atmospheric Correction for Remotely-Sensed Ocean Colour Products*; Wang, M., Ed.; Reports of the International Ocean-Colour Coordinating Group, No. 10; IOCCG: Darmouth, NS, Canada, 2010.
9. Hoepffner, N.; Zibordi, G. Remote Sensing of Coastal Waters. *Encycl. Ocean. Sci.* **2009**, 732–741. [CrossRef]
10. Gordon, H.G.; Morel, A. *Remote Assessment of Ocean Color for Interpretation of Satellite Visible Imagery: A Review*; Springer: New York, NY, USA, 1983; p. 114.
11. Renosh, P.; Doxaran, D.; Keukelaere, L.; Gossn, J. Evaluation of Atmospheric Correction Algorithms for Sentinel-2-MSI and Sentinel-3-OLCI in Highly Turbid Estuarine Waters. *Remote Sens.* **2020**, *12*, 1285. [CrossRef]
12. Warren, M.A.; Simis, S.G.H.; Martinez-Vicente, V.; Poser, K.; Bresciani, M.; Alikas, K.; Spyrakos, E.; Giardino, C.; Ansperd, A. Assessment of atmospheric correction algorithms for the Sentinel-2A MultiSpectral Imager over coastal and inland waters. *Remote Sens. Environ.* **2019**, *225*, 267–289. [CrossRef]
13. Pereira-Sandoval, M.; Ruescas, A.B.; Urrego, P.; Ruiz-Verdú, A.; Tenjo, C.; Soria-Perpinyà, X.; Vicente, E.; Soria, J.M.; Moreno, J. Evaluation of Atmospheric Correction Algorithms over Spanish inland waters for Sentinel-2 MSI data. *Remote Sens.* **2019**, *11*, 1469. [CrossRef]
14. Doerffer, R.; Schiller, H. The MERIS Case 2 water algorithm. *Int. J. Remote Sens.* **2007**, *28*, 517–535. [CrossRef]
15. Mobley, C.D. Estimation of the remote-sensing reflectance from above-surface measurements. *Appl. Opt.* **1999**, *38*, 7442–7455. [CrossRef] [PubMed]
16. European Space Agency, Sentinel-2 Spectral Response Functions (S2-SRF) v3.0. Available online: https://earth.esa.int/web/entinel/user-guides/sentinel-2-msi/document-library/-/asset_publisher/Wk0TKajiISaR/content/sentinel-2a-spectralresponses (accessed on 16 April 2020).
17. Shoaf, W.T.; Lium, B.W. Improved extraction of chlorophyll a and b from algae using dimethyl sulphoxide. *Limnol. Oceanogr.* **1976**, *21*, 926–928. [CrossRef]
18. Jeffrey, S.W.; Humphrey, G.F. New Spectrophotometric Equations for Determining Chlorophylls a, b, C1 and C2 in Higher Plants, Algae and Natural Phytoplankton. *Biochem. Physiol. Pflanz.* **1975**, *167*, 191–194. [CrossRef]
19. APHA. *Standard Methods for the Examination of Water and Wastewater*, 20th ed.; American Public Health Association: Washington, DC, USA, 1998.
20. Copernicus Open Access Hub. Available online: https://scihub.copernicus.eu/ (accessed on 27 September 2021).
21. SNAP. ESA Sentinel Application Platform v8.0. Available online: https://step.esa.int/main/download/snap-download/ (accessed on 27 September 2021).
22. Sentinel-2 MSI User Guide: Radiometric Resolutions. Available online: https://sentinel.esa.int/web/sentinel/user-guides/sentinel-2-msi/resolutions/radiometric (accessed on 27 September 2021).
23. Brockmann, C.; Doerffer, R.; Peters, M.; Stelzer, K.; Embacher, S.; Ruescas, A. Evolution of the C2RCC neural network for Sentinel 2 and 3 for the retrieval of ocean colour products in normal and extreme optically complex waters. In Proceedings of the Living Planet Symposium 2016, Prague, Czech Republic, 9–13 May 2016.
24. C2X-Complex. ESA Step Forum. Available online: https://forum.step.esa.int/t/c2x-complex/29392 (accessed on 27 September 2021).
25. Kanamitsu, M.; Ebisuzaki, W.; Woollen, J.; Yang, S.K.; Hnilo, J.J.; Fiorino, M.; Potter, G.L. NCEP-DOE AMIP-II Reanalysis (R-2). *Bull. Am. Meteorol. Soc.* **2002**, *83*, 1631–1643. [CrossRef]
26. NASA Goddard Space Flight Center, Ocean Ecology Laboratory, Ocean Biology Processing Group. Ancillary Meteorological Ocean Color Data, NASA OB.DAAC. 2018. Available online: https://disc.gsfc.nasa.gov/datasets/OMTO3_003/summary (accessed on 29 February 2019).
27. NASA Ocean Color Data. Available online: https://oceandata.sci.gsfc.nasa.gov (accessed on 27 September 2021).
28. Cui, T.; Zhang, J.; Groom, S.; Sun, L.; Smyth, T.; Sathyendranath, S. Validation of MERIS ocean-color products in the Bohai Sea: A case study for turbid coastal waters. *Remote Sens. Environ.* **2010**, *114*, 2326–2336. [CrossRef]

29. Müller, D.; Krasemann, H.; Brewin, R.J.W.; Brockmann, C.; Deschamps, P.Y.; Doerffer, R.; Fomferra, N.; Franz, B.A.; Grant, M.G.; Groom, S.B.; et al. The Ocean Colour Climate Change Initiative: I. A methodology for assessing atmospheric correction processors based on in situ measurements. *Remote Sens. Environ.* **2015**, *162*, 242–256. [CrossRef]
30. Poole, H.H.; Atkins, W.R.G. Photoelectric measurements of submarine illumination throughout the year. *J. Mar. Biol. Assoc. U. K.* **1929**, *16*, 297–324. [CrossRef]
31. Holmes, R. The Secchi disk in turbid coastal waters. *Limnol. Oceanogr.* **1970**, *15*, 688–694. [CrossRef]
32. Pahlevan, N.; Mangin, A.; Balasubramanian, S.V.; Smith, B.; Alikas, K.; Arai, K.; Barbosa, C.; Bélanger, S.; Binding, C.; Bresciani, M.; et al. ACIX-Aqua: A global assessment of atmospheric correction methods for Landsat-8 and Sentinel-2 over lakes, rivers, and coastal waters. *Remote Sens. Environ.* **2021**, *258*, 112366. [CrossRef]
33. Niroumand-Jadidi, M.; Bovolo, F.; Bruzzone, L.; Gege, P. Inter-Comparison of Methods for Chlorophyll-a Retrieval: Sentinel-2 Time-Series Analysis in Italian Lakes. *Remote Sens.* **2021**, *13*, 2381. [CrossRef]
34. Ligi, M.; Kutser, T.; Kallio, K.; Attila, J.; Koponen, S.; Paavel, B.; Soomets, T.; Reinart, A. Testing the Performance of Empirical Remote Sensing Algorithms in the Baltic Sea Waters with Modelled and in Situ Reflectance Data. *Oceanologia* **2017**, *59*, 57–68. [CrossRef]
35. Tavares, M.H.; Lins, R.C.; Harmel, T.; Fragoso, C.R.; Martínez, J.M.; Motta-Marques, D. Atmospheric and sunglint correction for retrieving chlorophyll-a in a productive tropical estuarine-lagoon system using Sentinel-2 MSI imagery. *ISPRS J. Photogramm. Remote Sens.* **2021**, *174*, 215–236. [CrossRef]
36. Soomets, T.; Uudeberg, K.; Jakovels, D.; Brauns, A.; Zagars, M.; Kutser, T. Validation and comparison of water quality products in baltic lakes using sentinel-2 msi and sentinel-3 OLCI data. *Sensors* **2020**, *20*, 742. [CrossRef] [PubMed]
37. Uudeberg, K.; Ansko, I.; Põru, G.; Ansper, A.; Reinart, A. Using optical water types to monitor changes in optically complex inland and coastal waters. *Remote Sens.* **2019**, *11*, 2297. [CrossRef]
38. Ansper, A.; Alikas, K. Retrieval of chlorophyll a from Sentinel-2 MSI data for the European Union water framework directive reporting purposes. *Remote Sens.* **2019**, *11*, 64. [CrossRef]
39. Spyrakos, E.; O'Donnell, R.; Hunter, P.D.; Miller, C.; Scott, M.; Simis, S.G.H.; Neil, C.; Barbosa, C.C.F.; Binding, C.E.; Bradt, S.; et al. Optical types of inland and coastal waters. *Limnol. Oceanogr.* **2018**, *63*, 846–870. [CrossRef]
40. Moore, T.S.; Dowell, M.D.; Bradt, S.; Ruiz-Verdú, A. An optical water type framework for selecting and blending retrievals from bio-optical algorithms in lakes and coastal waters. *Remote Sens. Environ.* **2014**, *143*, 97–111. [CrossRef]
41. Sòria-Perpinyà, X.; Vicente, E.; Urrego, P.; Pereira-Sandoval, M.; Tenjo, C.; Ruíz-Verdú, A.; Delegido, J.; Soria, J.M.; Peña, R.; Moreno, J. Validation of water quality monitoring algorithms for sentinel-2 and sentinel-3 in Mediterranean inland waters with in situ reflectance data. *Water* **2021**, *13*, 686. [CrossRef]
42. Caballero, I.; Fernández, R.; Escalante, O.M.; Mamán, L.; Navarro, G. New capabilities of Sentinel-2A/B satellites combined with in situ data for monitoring small harmful algal blooms in complex coastal waters. *Sci. Rep.* **2020**, *10*, 1–14. [CrossRef]
43. Gons, H.J.; Rijkeboer, M.; Ruddick, K.G. Effect of a waveband shift on chlorophyll retrieval from MERIS imagery of inland and coastal waters. *J. Plankton Res.* **2005**, *27*, 125–127. [CrossRef]
44. Gitelson, A.A.; Dall'Olmo, G.; Moses, W.; Rundquist, D.C.; Barrow, T.; Fisher, T.R.; Gurlin, D.; Holz, J. A simple semi-analytical model for remote estimation of chlorophyll-a in turbid waters: Validation. *Remote Sens. Environ.* **2008**, *112*, 3582–3593. [CrossRef]
45. Mishra, S.; Mishra, D.R. Normalized difference chlorophyll index: A novel model for remote estimation of chlorophyll-a concentration in turbid productive waters. *Remote Sens. Environ.* **2012**, *117*, 394–406. [CrossRef]
46. Nechad, B.; Ruddick, K.G.; Park, Y. Calibration and validation of a generic multisensor algorithm for mapping of total suspended matter in turbid waters. *Remote Sens. Environ.* **2010**, *114*, 854–866. [CrossRef]
47. Gernez, P.; Lafon, V.; Lerouxel, A.; Curti, C.; Lubac, B.; Cerisier, S.; Barillé, L. Toward sentinel-2 high resolution remote sensing of suspended particulate matter in very turbid waters: SPOT4 (take5) experiment in the Loire and Gironde estuaries. *Remote Sens.* **2015**, *7*, 9507–9528. [CrossRef]
48. Alvado, B.; Sòria-Perpinyà, X.; Vicente, E.; Delegido, J.; Urrego, P.; Ruíz-Verdú, A.; Soria, J.M.; Moreno, J. Estimating Organic and Inorganic Part of Suspended Solids from Sentinel 2 in Different Inland Waters. *Water* **2021**, *13*, 2453. [CrossRef]